processes

MDPI

Article

The Stopping Performance of a Centrifugal Pump with Splitter Blades at Small Discharge Valve Openings

Xin Li [1], Jiang-Bo Tong [2], Xiao-Wei Xu [1,*] and Yu-Liang Zhang [1,*]

[1] Zhejiang Key Laboratory of Intelligent Manufacturing for Aerodynamic Equipment, College of Mechanical Engineering, Quzhou University, Quzhou 324000, China
[2] School of Mechanical Engineering, Hunan University of Technology, Zhuzhou 412007, China
* Correspondence: 36084@qzc.edu.cn (X.-W.X.); zhang002@sina.com (Y.-L.Z.)

Abstract

To reveal the hydraulic characteristics of a centrifugal pump with splitter blades during shutdown, a low specific speed closed impeller centrifugal pump is subjected to shutdown experiments under eight non-rated operating conditions in this paper. The transient evolution characteristics of five performance parameters with time are obtained, including rotational speed, flow rate, inlet and outlet pressures, and head. Meanwhile, the shutdown fitting models based on three machine learning models are developed. The results show that the integrated neural network model can more accurately predict the hydraulic performance of the physical pump during shutdown than the decision tree regression and random forest regression models. During the pre-mid period of the shutdown, the integrated neural network model predicts a maximum error of about 3.21% for the instantaneous flow rate and about 3.58% for the instantaneous head. This study provides a reference for the performance control of centrifugal pumps during transient operation.

Keywords: centrifugal pump; shutdown; performance experiments; machine learning

check for updates

Academic Editor: Krzysztof Rogowski

Received: 28 August 2025
Revised: 29 September 2025
Accepted: 10 October 2025
Published: 12 October 2025

Citation: Li, X.; Tong, J.-B.; Xu, X.-W.; Zhang, Y.-L. The Stopping Performance of a Centrifugal Pump with Splitter Blades at Small Discharge Valve Openings. *Processes* **2025**, *13*, 3243. https://doi.org/10.3390/pr13103243

Copyright: © 2025 by the authors. Licensee MDPI, Basel, Switzerland. This article is an open access article distributed under the terms and conditions of the Creative Commons Attribution (CC BY) license (https://creativecommons.org/licenses/by/4.0/).

1. Introduction

Centrifugal pumps, as versatile fluid transfer devices, are widely used in metallurgy and coal, petroleum and chemical, agricultural irrigation, and other fields [1–3]. Under steady state operation, the internal fluid flow is smooth, and the performance parameters remain relatively constant, so conventional applications and studies are mainly concerned with the steady state characteristics. However, compared with the steady state study of fluid mechanics [4–8], the study of transient processes (e.g., pump startup and shutdown periods) is more complex. In the transition process of pump startup and shutdown, the performance parameters will change dramatically in a very short period of time, the internal energy conversion is rapid and complex, and it is very easy to induce water hammer impact and other hazards, which seriously threaten the safety of pump unit operation [9,10]. Therefore, in-depth grasping the transient parameter change rule of centrifugal pump during startup and shutdown has important engineering practice significance for effectively improving the operation safety.

So far, a number of researchers have carried out investigations into the transient characteristics of pumps under startup conditions. Tsukamoto et al. experimentally found that the pressure pulsation and the delay of the blade annulus during normal startup are the main factors leading to the difference between transient and quasi-steady state [11]. Wang et al. simulated the startup process of a centrifugal pump using a dynamic mesh

and qualitatively revealed the existence mechanism of the transient effect [12]. Tanaka et al. revealed that the coupling effect of impeller acceleration and fluid inertia force during rapid startup is the main cause of pressure fluctuation through transparent pump experiments and CFD simulations [13–15]. Lefebvre et al. demonstrated through mixed-flow pump acceleration experiments that the quasi-steady state assumption exhibits limitations in predicting transient performance [16]. Wu et al. showed that the transient characteristics at the early stage of startup are particularly significant through the rapid startup tests [17]. Xu et al. developed a numerical model for a high-power centrifugal pump under startup and confirmed that the sudden change in head is related to the anomaly of the axial thrust [18]. Dazin et al. proposed that acceleration, flow rate, and flow field evolution processes all exert a significant influence on the associated transient effects [19]. Dong et al. confirmed that the linear acceleration scheme can significantly inhibit the development of a vortex in the flow channel through the ultrashort startup experiments [20]. Chen et al. established a correction formula for the head for the unsteady condition through the startup experiments with variable valve opening [21]. Yun et al. discovered that the transient excitation force during closed-valve startup of multistage pumps was higher than that of conventional pumps [22]. Hu et al. found that the rapid startup of centrifugal pumps exhibits pronounced transient effects only during the initial phase relative to the quasi-steady state assumption, subsequently converging to steady-state performance [23].

Similarly, for the pump shutdown period, there have been many researchers have conducted investigations to investigate the flow characteristics of many types of pumps during shutdown and the effects of shutdown conditions, shutdown schemes, and conveyed fluids on the shutdown characteristics. Zhang et al. confirmed that the similarity law can predict the hydraulic performance of low-speed shutdown under a small flow rate based on the no-measurement analysis and quasi-steady state method [24]. Shourkaei showed through theoretical study that the flow rate of the shutdown period decays nonlinearly with respect to the speed, and the decay rate during the initial period is larger than that during the later period [25]. Ma et al. found that the head of quasi-steady state is significantly higher than the transient value when the hybrid pump is shut down based on CFD and theoretical study [26]. Liu simulated the transient characteristics of a radial flow pump under fast shutdown [27]. Feng et al. developed an iterative algorithm for the angular momentum equation, and the outer characteristic curve of the runaway parameter from numerical simulation was highly consistent with the experiment [28]. Liu et al. introduced a novel CFD methodology, which was experimentally verified and found to accurately simulate the shutdown flow in an axial flow pump system [29]. Zhang et al. found that the liquid viscosity is negatively correlated with the transient response, and the pump shutdown response is faster with high viscosity fluids [30]. Wu et al. confirmed that pipeline fluid inertia leads to transient pressure overshooting at the inlet and outlet of the pump, and the performance curves deviate from the steady state [31]. Zhang et al. showed experimentally that the valve opening significantly affects the parameters evolution, including shutdown speed and head, of the open-impeller centrifugal pump [32]. Zhang et al. also explored the impact of downtime on the transient performance for five non-inertial shutdown conditions [33]. Kan et al. found that when a tubular pump loses control at a power outage, the head and flow rate will be drastically decayed, and the full domain of the flow regime will be reconstructed [34].

Taken together, extensive research has been conducted by researchers on pump startup and shutdown. However, these studies have been limited to performance experiments, and performance prediction studies using, for example, machine learning, have not been addressed in depth. Current studies on the prediction of hydraulic performance of centrifugal pumps are also limited to steady state conditions [35–37]. Based on this, the transient perfor-

mance of a low specific speed centrifugal pump with splitter blades under eight non-rated operating conditions is experimentally obtained, and the evolution rules of parameters such as speed and head are obtained. At the same time, the hydraulic performances of the pump during shutdown are predicted based on three models, namely, decision tree regression, random forest regression, and an integrated neural network, and the prediction accuracies of the three machine learning models for hydraulic performances are also evaluated.

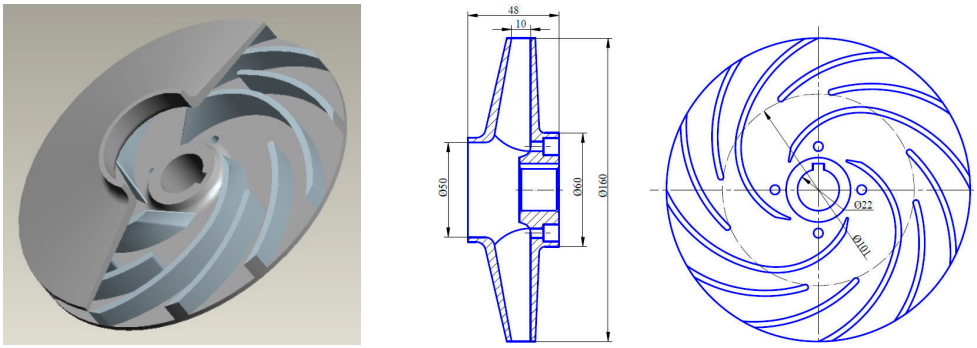
2. Test Pump and Test Rig

2.1. Test Pump

The test pump is a low-specific-speed (n_s = 45), closed-impeller centrifugal pump designed for a flow rate of 6 m^3/h, a head of 8 m, and a rotational speed of 1450 r/min, with its main geometrical parameters provided in Table 1. And the impeller has 4 long blades and 8 short blades, that is, 8 splitter blades, as shown in Figure 1.

Table 1. The main parameters of the test pump.

Test Pump	
Diameter of suction D_i/mm	50
Diameter of discharge D_o/mm	40
Blade number Z	12
Blade inlet angle β_1/°	25
Blade outlet angle β_1/°	25
Diameter of impeller inlet D_1/mm	48
Diameter of impeller outlet D_2/mm	160
Width of blade inlet b_1/mm	20
Width of blade outlet b_2/mm	10
Basic diameter of volute D_3/mm	165
Width of volute inlet b_3/mm	15
Diameter of volute throat Dth/mm	15
Thickness of blade δ/mm	3



(**a**) Internal structure (**b**) Main dimensions (mm)

Figure 1. Impeller of test centrifugal pump.

2.2. Test Rig

The test bench for external characteristic transient performance of centrifugal pump constructed in this experiment is consistent with the literature [38,39], as shown in Figure 2. The instantaneous flow rate was measured using an OPTIFLUX 2100C electromagnetic flowmeter supplied by KROHNE (Shanghai, China) Co., Ltd. This instrument features an output signal of 4~20 mA, a time constant of 0.1 s, a pulse output frequency of 1 kHz, a maximum measurable flow rate of 30 m^3/h, and an accuracy class of 0.5. The instantaneous pressures at the pump inlet and outlet were measured using pressure transmitters from WIKA, Klingenberg am Main, Germany. The pressure sensor at the pump inlet has a

measurement range of −0.1~0.1 MPa, while the sensor at the outlet covers a range of 0.0~1.6 MPa. Both sensors operate at a supply voltage of 10~30 VDC, provide a 4~20 mA output signal, and offer an accuracy of 0.25%. The instantaneous rotational speed of the centrifugal pump was acquired using a JCO-type torque-speed sensor manufactured by Hunan Xiangyi Power Testing Instrument Co., Ltd., Changsha, China, with a rated torque of 5.0 N·m and a speed measurement range of 0~6000 rpm. The motor speed was regulated by a SIEMENS MICROMASTER 440 frequency converter from Munich, Germany, which adjusts the electrical supply frequency. Data acquisition was performed using a PCI8361BN data acquisition card produced by Beijing Zhongtai Yanchuang Technology Co., Ltd., Beijing, China. The experiments are conducted by controlling the ball valve opening on the outlet line to achieve steady flow control, defining the relative flow rate as the ratio of actual flow rate to designed flow rate (Q/Q_r). The desired predetermined relative flow rates are 0.2, 0.3, 0.4, 0.5, 0.6, 0.7, 0.8, and 0.9 for each of the eight different valve openings for the shutdown experiments.

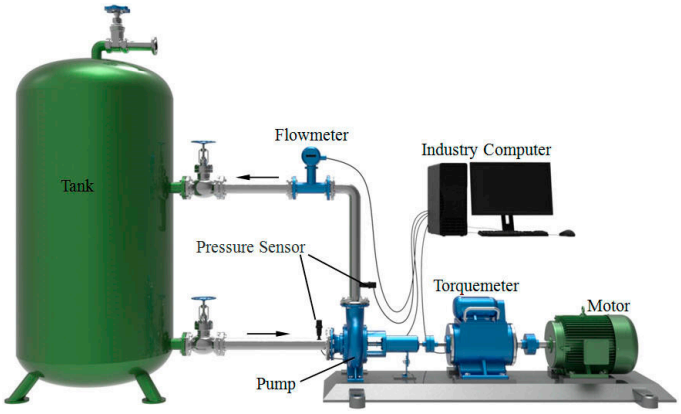


Figure 2. Schematic diagram of test bench.

In the previous study [39], the authors conducted transient performance experiments on the shutdown process of the same pump under direct-on-line (DOL) mode (where the motor is started directly without controlling the current frequency, and then is stopped). For the physical pump in this study, shutdown experiments would be carried out under variable frequency drive (VFD) mode (where motor speed is regulated by controlling the power supply frequency).

3. Experimental Results

Based on the aforementioned experimental rig, the study successfully obtained the evolution patterns of external characteristic parameters during the shutdown transient process of a low specific speed closed impeller centrifugal pump, specifically including parameters such as rotational speed, flow rate, inlet and outlet pressure, and head.

The impeller speed changes during shutdown of the experimental pump are shown in Figure 3. It shows that the target relative flow rates in this study are set at 0.2, 0.3, 0.4, 0.5, 0.6, 0.7, 0.8, and 0.9. However, experimental results showed that the actual relative flow rates are 0.206, 0.295, 0.406, 0.503, 0.609, 0.697, 0.797, and 0.891 in the process of shutdown. In the previous DOL mode study [39], although the target relative flow rates also included four cases (0.2, 0.4, 0.6, and 0.8), the measured values are 0.213, 0.418, 0.616, and 0.820, respectively.

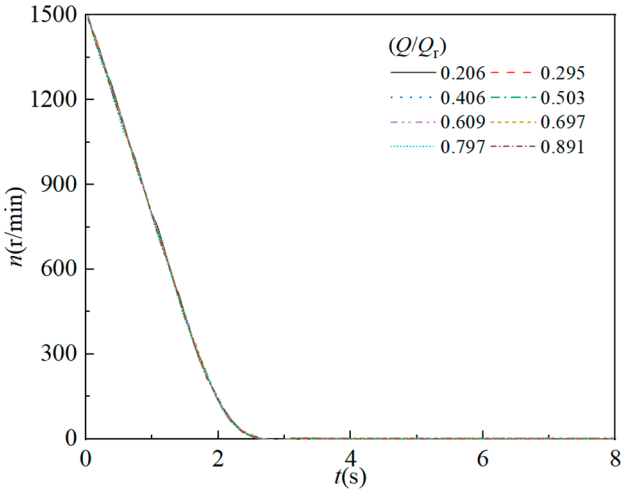


Figure 3. Speed characteristics during shutdown.

During the pump shutdown process, all speed curves exhibit a tendency to decline rapidly initially, followed by a gradual decrease. For Q/Q_r = 0.503, the impeller speed plummets from 1495 r/min (pre-shutdown) to 61 r/min from approximately 0 s to 2.22 s; and it then gradually decreases to 0 r/min from approximately 2.22 s to 2.70 s. This indicates a very rapid speed response to the pump shutdown. In pump shutdown processes, the rotational speed curves under different flow rate conditions are nearly identical, showing negligible differences. This is primarily because the shutdown tests are conducted in frequency conversion mode: the impeller speed at each flow rate is determined by the motor speed, which in turn is controlled by the inverter-set frequency, and the influence of hydraulic resistance on impeller speed is minimal, hence the negligible differences in the speed curves. However, under the DOL (direct-on-line) mode [39], it shows that during the shutdown process, the speed decay curves exhibit significant differences under varying valve openings (i.e., different relative flow rates).

The flow rate changes during shutdown are shown in Figure 4. It can be observed that during the pump shutdown process, the flow rate consistently exhibits a trend of first maintaining relative stability, followed by a slow decrease, and then a rapid drop. Such as Q/Q_r = 0.797, about from 0 s to 1.06 s, the flow rate maintains stability; and then about from 1.06 s to 6.42 s, the flow rate from 4.76 m^3/h slowly down to 0.42 m^3/h; and finally about from 6.42 s to 7.24 s, the flow rate down to zero, the rate of decline is significantly greater. And by other flow rate conditions can be found, all flow rates can also maintain a period of stability at the beginning of the shutdown. The reason for this is that, although the speed decreases during frequency conversion shutdown, the motor continues to rotate autonomously and turns the impeller, which has a certain effect on maintaining a stable flow rate. In addition, the flow rate can also be maintained for a short period of time, also affected by the flow inertia.

It is also found that overall, the time required to complete shutdown grows with increasing valve opening. During the pump shutdown period, the flow rate to zero time at Q/Q_r = 0.206, 0.295, 0.406, 0.503, 0.609, 0.697, 0.797, and 0.891 is about 4.86 s, 5.27 s, 5.63 s, 4.20 s, 6.19 s, 6.42 s, 7.24 s, and 7.64 s, respectively. It can be seen that as the flow rate increases, there is an overall increase in the time to complete shutdown.

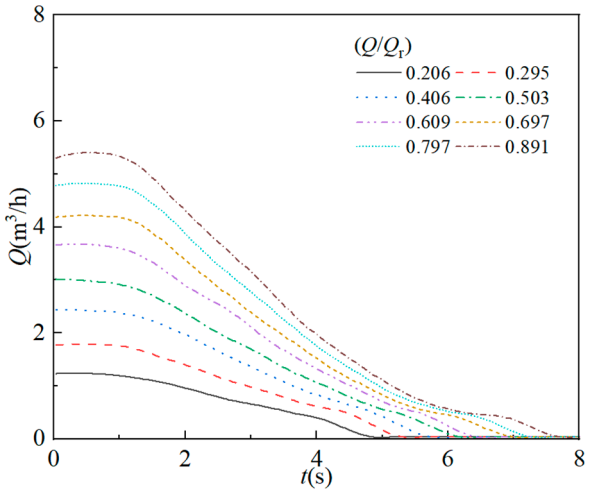


Figure 4. Flow rate characteristics during shutdown.

The inlet pressure changes during shutdown are shown in Figure 5. It is evident that the variations in inlet pressure under different flow rate ratios exhibit marked differences. At the beginning of the shutdown, the inlet pressure rises slowly and then decreases slowly at Q/Q_r = 0.206, 0.295, 0.406, and 0.503. While at larger flow rate ratios Q/Q_r = 0.609, 0.697, 0.797, and 0.891, the inlet pressure first rises and then falls. The pressure changes in the larger flow rate ratio scenarios are all more drastic. It is found that the inlet pressure under small flow rate ratios, Q/Q_r = 0.206 and 0.295, fluctuates steadily and is relatively stable, while under other conditions of larger flow rate ratios, the inlet pressure shows a tendency to rise and then fall, and the phenomenon is more obvious with increasing flow rate ratio. However, at the end of the shutdown, with the impeller speed decreasing and stopping rotating, the inlet pressure under each flow rate tends to be the same steady value, about 6.77 kPa.

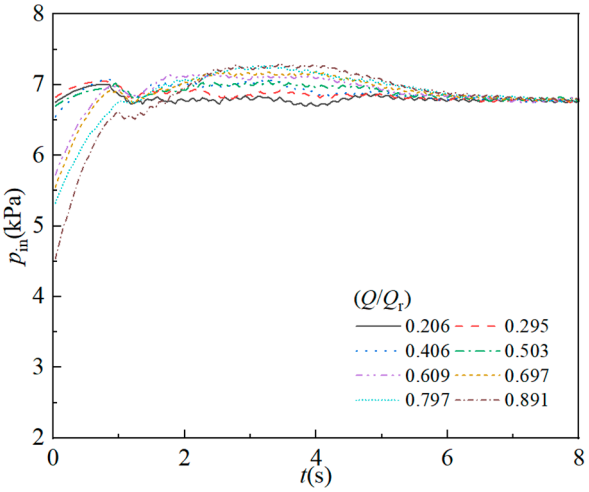


Figure 5. Inlet pressure characteristics during shutdown.

The outlet pressure changes during shutdown are shown in Figure 6. It shows that the outlet pressure curves at each flow rate show a rapid decrease to a stable value. Taking Q/Q_r = 0.609 as an example, from about 0 s to 4.18 s, the outlet pressure decreases rapidly from 112.97 kPa to 11.11 kPa; after that, the outlet pressure remains relatively stable. It also shows that under the shutdown, the outlet pressures reach a stable value at about the same time, about t = 4.18 s. It indicates that the valve opening prior to shutdown has almost no effect on the time when the outlet pressure tends to stabilize.

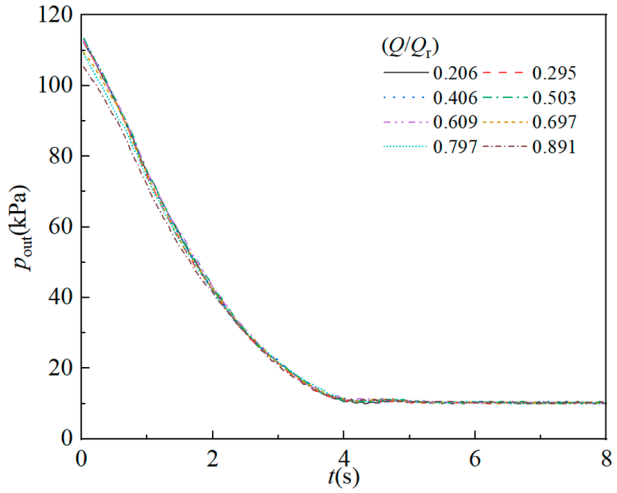


Figure 6. Outlet pressure characteristics during shutdown.

The head changes during shutdown are shown in Figure 7. By comparing Figures 6 and 7, it can be observed that the head curve and the outlet pressure curve exhibit essentially identical characteristics, indicating that the variation trend and magnitude of the head are primarily determined by the outlet pressure. During the shutdown of Q/Q_r = 0.609, from 0 s to 4.18 s, the head rapidly decreases from 10.97 m to 0.42 m; after that, the head also remains relatively stable, with the same change characteristics of outlet pressure.

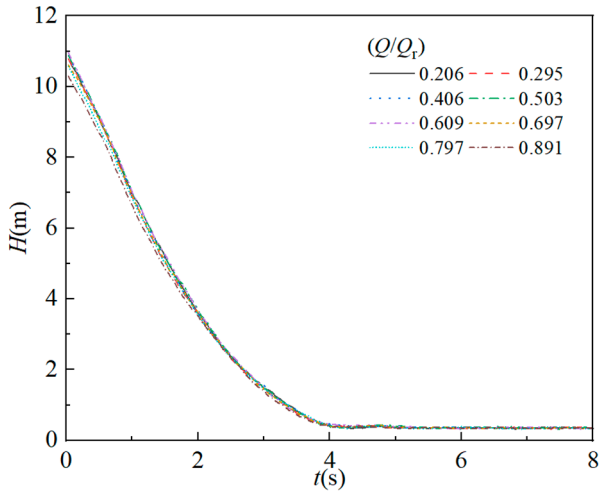


Figure 7. Head characteristics during shutdown.

In addition, under different flow rate ratios, the stabilization times for head and outlet pressure are essentially identical. This is primarily because the outlet pressure of the centrifugal pump is significantly higher than the inlet pressure, and the absolute value of the inlet pressure is relatively small. Consequently, changes in head are predominantly determined by variations in outlet pressure. Therefore, during shutdown, the variation characteristics of head and outlet pressure are highly consistent at the same flow ratio.

4. Performance Prediction

Three machine learning models, namely decision tree regression, random forest regression, and integrated neural network, are used in this paper to fit the external characteristic curves of the experimental pump, and the reliability of the three prediction models is also evaluated. The fitted training set uses the external characteristic sample

curves at Q/Q_r = 0.206, 0.295, 0.406, 0.503, 0.697, 0.797, and 0.891 for the pump shutdown experiments, and the external characteristic sample curves with steady flow rate ratio Q/Q_r = 0.609 for the pump shutdown experiment are used as the test sets to validate the corresponding prediction results of the three models.

4.1. Prediction Models

As a classical machine learning model, the decision tree regression model is based on the decision tree structure to predict continuous values of the target variable by recursively partitioning the feature space [40,41]. In the process of making decisions, it can gradually divide the data into smaller and more similar subsets to form a tree structure. And its tree structure is intuitive, the decision rules are clear and easy to understand, and it can deal with many data types and nonlinear relationships. Its model structure is transparent and highly interpretable, capable of intuitively visualizing the decision paths from input features (e.g., time, operating conditions) to output targets (e.g., flow rate, head). The steps of learning to predict are as follows:

(1) For each node R, minimize the squared error of its internal samples:

$$MSE(R) = \frac{1}{N_R}\sum_{i=1}^{n}(y_i - \overline{y})^2 \tag{1}$$

(2) For feature j and split point s, calculate the error reduction after splitting, and choose the (j, s) split with the largest $Gain(j, s)$

$$Gain(j,s) = MSE(R) - \left(\frac{N_{R_L}}{N_R}MSE(R_L) + \frac{N_{R_R}}{N_R}MSE(R_R)\right) \tag{2}$$

(3) The predicted value of the leaf node R_m is the sample mean for the region:

$$\hat{y}_m = \overline{y}_{R_m} \tag{3}$$

where N_R is the sample number of the current node; N_{R_L} and N_{R_R} are the sample numbers of the left and right child nodes; y_i is the actual observation; $\overline{y}$ is the mean of the sample actual values; $MSE(R)$ is the mean-square error of the current node; $MSE(R_L)$ and $MSE(R_R)$ are the mean-square errors of the left and right child nodes.

The random forest regression model [42–44] is a regression algorithm based on integrated learning and Bootstrap Aggregating techniques. By constructing multiple decision trees and integrating their results, it effectively mitigates the overfitting tendency inherent in individual decision trees, significantly enhances the model's generalization capability and predictive stability, and ensures relatively reliable prediction accuracy even under unseen transient operating conditions. Mathematically, it can be summarized as follows: given data samples X and prediction set Y, on top of which forests dependent on random variable θ are planted, constituting a tree predictor $h(x, \theta_k)$, which outputs numerical values, and a random forest predictor is obtained by taking the mean of these trees $\{h(x, \theta_k)\}$ with respect to k. The set of samples obeying the distribution of random variables Y, X and drawn independently is taken as the training set, and the mean-square generalization error of any tree predictor $h(X)$ is $E_{X,Y}(Y - h(X))^2$. When the number of trees in the forest increases infinitely, everywhere:

$$E_{X,Y}(Y - av_k h(X, \theta_k))^2 \to E_{X,Y}(Y - E_\theta h(X, \theta))^2 \tag{4}$$

Then, the regression function of the random forest is: $Y = E_\theta h(X, \theta)$, which is often used in place of the approximate formula when k is sufficiently large: $Y = av_k h(X, \theta_k)$. At this point, the error is analyzed as below:

$$PE^*(\text{tree}) = E_\theta E_{X,Y}(Y - h(X, \theta))^2 \quad (5)$$

where the average generalization error of the random forest is denoted by $PE*$.

Neural networks are well-suited for fitting complex temporal variation patterns of parameters such as flow rate and head during shutdown processes, owing to their powerful function approximation capabilities. The integrated neural network, as an ensemble learning method, further reduces model variance and enhances the robustness and accuracy of predictions by combining the outputs of multiple relatively weak base models [45,46]. Different from the random forest regression model, which is usually based on a single type of base learner and builds diversity randomly, the core difference in integrated neural networks lies in the heterogeneity of their base models. Specifically, the method independently trains multiple neural network models with different initializations of structure or parameters and fuses the predictions through an integration strategy to obtain higher prediction accuracy than a single model. However, due to the need to train and maintain several models, integrated neural networks usually require a higher computational cost and model complexity.

4.2. Prediction Results

The flow rate and head are two important performance parameters of a centrifugal pump. In this study, considering the complex evolution of flow rate and head curves during pump shutdown, the instantaneous flow rate and head under shutdown are fitted and predicted based on the decision tree regression, random forest regression, and integrated neural network models.

After the models are trained and calculated, the instantaneous flow rate prediction results are shown in Figure 8 for pump shutdown at Q/Q_r = 0.609. It can be seen that the integrated neural network model predicts the transient flow rate at shutdown most accurately, and only the prediction at the end of shutdown has a large deviation. At the end of the shutdown period from t = 4.73 s to t = 8.0 s, the maximum deviation occurs around t = 6.13 s, approximately 0.14 m^3/h. During the pre-mid period of the shutdown from t = 0 s to t = 4.73 s, both the maximum deviation value and maximum error occur around t = 2.61 s, with a maximum deviation of about 0.08 m^3/h and a maximum error of about 3.21%.

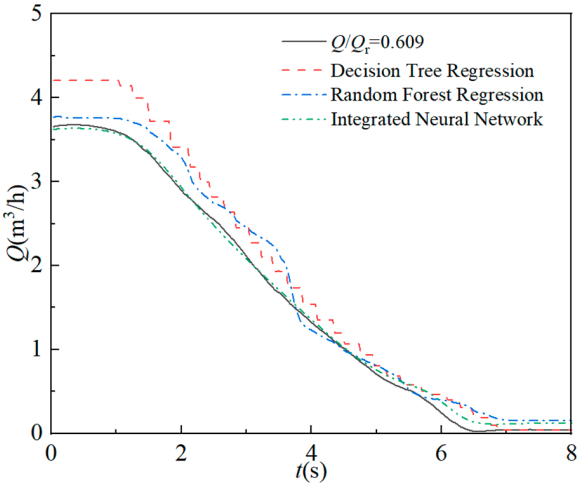


Figure 8. Prediction of flow rate during shutdown.

For the other two models, it is also found that the two prediction curves deviate significantly from the experimental data, and both curves in the middle of the shutdown period show a fluctuating decrease, and the variation trend is not consistent with the experimental curves. In summary, the predictions by the integrated neural network model are more credible in the instantaneous flow prediction during the whole shutdown process.

The instantaneous head prediction results are shown in Figure 9 for pump shutdown at $Q/Q_r = 0.609$. Overall, the prediction curves of the instantaneous head of the decision tree regression and integrated neural network models are in good agreement with the experimental curves, with consistent trends and small deviations. Only in the early stage of shutdown from $t = 0$ s to $t = 0.36$ s, the decision tree regression model predicts significant deviations, with a maximum deviation of about 0.58 m and a maximum error of about 5.28%. In contrast, for the integrated neural network model, during the pre-mid period of the shutdown from $t = 0$ s to $t = 3.52$ s, the maximum deviation is about 0.10 m and the maximum error is about 3.58%.

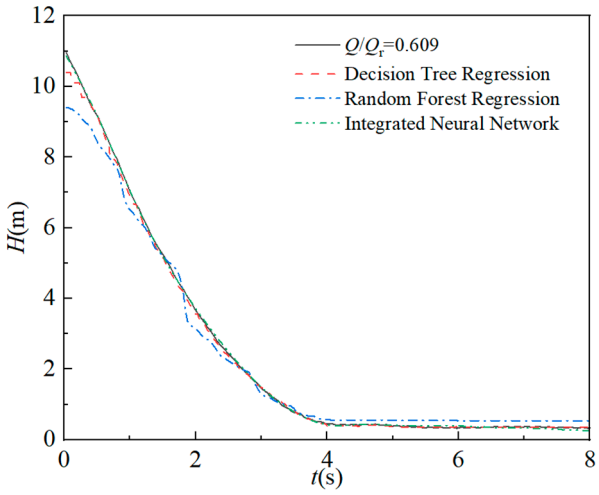


Figure 9. Prediction of pump head during shutdown.

For the random forest regression model, it is found that during pump shutdown, the head prediction curve shows a fluctuating decline, with a large difference in the trend of the experimental curve, and the final prediction head of complete shutdown is also larger than the experimental head of about 0.20 m. It is clear that the established random forest regression model cannot predict the head during pump shutdown periods more accurately, and the credibility of the predicted data is low.

4.3. Discussion

(1) After the shutdown, the head curve is still greater than 0; the reason for this phenomenon is the inlet and outlet pressure sensor installation location. In this test, the inlet pressure sensor was mounted vertically upwards on the branch pipe of the pump inlet pipeline, and the outlet pressure sensor was mounted vertically downwards on the branch pipe of the pump outlet pipeline, thus making the two up and down positions different, and the free liquid level in the tank is higher than the two pressure sensors. The adjustment and optimization of installation locations of pressure sensors are the next step in the working direction.

(2) For the current test devices, the ranges of the various types of sensors used in the test are generally large, resulting in a decline in the accuracy and precision of the measured values, and a large error in parameter fluctuations. The maximum range of the electromagnetic flowmeter is 30 m^3/h, while the designed flow rate of the model pump is only 6 m^3/h. The ranges of the inlet and outlet pressure sensors are

−0.1~0.1 MPa and 0.0~1.6 MPa, respectively, which are much larger than the actual pressure. Therefore, the ranges of the current test instruments need to be further optimized in order to obtain more accurate and reliable measurement results.

(3) There is a lack of synchronization in the sampling time of the main parameters. This is mainly due to the different sampling frequencies of individual sensors and signal transmission differences, which is the focus of the next work.

(4) This study has certain experimental limitations. Firstly, the current work primarily focuses on capturing the macroscopic evolution patterns of the external characteristic parameters of the centrifugal pump during transient processes, while the underlying transient flow mechanisms have not been revealed through internal flow field measurements. Secondly, as multiple repeated experiments were not conducted, error analysis of the measurement results could not be performed. In future studies, flow diagnostic techniques such as Particle Image Velocimetry (PIV) or high-speed photography could be employed to further investigate the evolution of internal flow structures. Additionally, multiple repeated experiments should be conducted to enhance data reliability.

(5) The conclusions drawn in this study regarding the transient evolution characteristics and the predictive performance of the machine learning models are strictly derived from the specific low specific speed closed impeller centrifugal pump employed in the current experiments, along with the transient dataset acquired under the defined eight shutdown non-rated operating conditions. It must be emphasized that these findings may not be directly generalizable to impellers with significantly different geometries, those subject to geometric alterations due to long-term operation involving cavitation, wear, or corrosion, or to different operational media and environments. And this limitation concurrently reveals opportunities for subsequent research: future work could focus on incorporating time-varying geometric evolution factors of the impeller and expanding the operational range to validate and enhance the universality and robustness of such machine learning models in practical engineering applications.

In spite of these, the test results presented herein have a great deal of significance for grasping the change rule of a single performance parameter of a composite impeller centrifugal pump during and shutdown.

5. Conclusions

(1) Compared with the random forest regression and decision tree regression models, the integrated neural network model is the most accurate for predicting the two key performance parameters during pump shutdown, and the prediction curves are highly consistent with the experimental curves. During the pre-mid period of the shutdown, the maximum prediction error of the integrated neural network model for the instantaneous flow rate and instantaneous head is about 3.58%.

(2) After the accuracy validation, it is found that the shutdown condition fitting models based on decision tree regression, random forest regression and integrated neural network can predict the hydraulic performance under shutdown, and the trend of the overall hydraulic performance curves under the predicted scenarios is generally consistent with the experimental curves, which can reflect a more realistic shutdown characteristics of the centrifugal pump with splitter blades.

(3) With increasing valve opening, the overall time taken to complete shutdown shows a tendency to lengthen. The speed and head decrease rapidly at the beginning of shutdown.

Author Contributions: Investigation, X.L.; writing—review and editing, J.-B.T.; Conceptualization, X.-W.X.; Investigation and supervision, Y.-L.Z. All authors have read and agreed to the published version of the manuscript.

Funding: The research was financially supported by the Science and Technology Project of Quzhou (No. 2024K147).

Data Availability Statement: The raw data supporting the conclusions of this article will be made available by the authors on request.

Conflicts of Interest: The authors declare no conflict of interest.

References

1. Zhang, L.; Wang, X.; Wu, P.; Huang, B.; Wu, D. Optimization of a centrifugal pump to improve hydraulic efficiency and reduce hydro-induced vibration. *Energy* **2023**, *268*, 126677. [CrossRef]
2. Nossir, E.F.E.; Elkelawy, M.; Bastawissi, H.A.E.; Elsamadony, M.O. A comprehensive review and background on centrifugal pump performance under multiphase flow and varying operating conditions. *Pharos Eng. Sci. J.* **2025**, *2*, 117–128. [CrossRef]
3. Lu, Y.; Tan, L. Design method based on a new slip-diffusion parameter of centrifugal pump for multiple conditions in wide operation region. *Energy* **2024**, *294*, 130796. [CrossRef]
4. Lu, J.; Liu, J.; Qian, L.; Liu, X.; Yuan, S.; Zhu, B.; Dai, Y. Investigation of pressure pulsation induced by quasi-steady cavitation in a centrifugal pump. *Phys. Fluids* **2023**, *35*, 025119. [CrossRef]
5. Liu, Y.; Tan, L. Spatial–temporal evolution of tip leakage vortex in a mixed-flow pump with tip clearance. *J. Fluids Eng.* **2019**, *141*, 081302. [CrossRef]
6. Meakhail, T.A.; Salem, M.; Shafie, I. Steady and unsteady flow inside a centrifugal pump for two different impellers. *Int. J. Energy Power Eng.* **2014**, *3*, 65–76. [CrossRef]
7. Jia, X.Q.; Shen, S.J.; Zhang, S.K.; Lv, H.; Lin, Z.; Zhu, Z. Influence of tip clearance on internal energy loss characteristics of axial flow pumps under different operating conditions. *Phys. Fluids* **2024**, *36*, 015102. [CrossRef]
8. Kan, K.; Yang, Z.; Lyu, P.; Zheng, Y.; Shen, L. Numerical study of turbulent flow past a rotating axial-flow pump based on a level-set immersed boundary method. *Renew. Energy* **2021**, *168*, 960–971. [CrossRef]
9. Liu, M.Q.; Liang, X.; Liu, Z.Y.; Lin, Q. Field measurement of water hammer and signal analysis at pump-stop due to power failure in long water-supply pipeline. *J. Drain. Irrig. Mach. Eng.* **2012**, *30*, 249–253. [CrossRef]
10. Huang, Y.Y.; Li, J.G.; Fu, X.Q.; Jiang, J.; Lan, G.; Fan, Z. Research on the comparison of air vessel and air valve on pump stopping water hammer protection of long-distance pipeline. *China Rural. Water Hydropower* **2014**, *8*, 186–188, 192.
11. Tsukamoto, H.; Ohashi, H. Transient characteristics of a centrifugal pump during starting period. *J. Fluids Eng.* **1982**, *104*, 6–13. [CrossRef]
12. Wang, L.Q.; Li, Z.F.; Dai, W.P.; Wu, D.Z. 2-D numerical simulation on transient flow in centrifugal pump during starting period. *J. Eng. Thermophys.* **2008**, *29*, 1319–1322.
13. Tanaka, T.; Tsukamoto, H. Transient behavior of a cavitating centrifugal pump at rapid change in operating conditions—Part 1: Transient phenomena at opening/closure of discharge valve. *J. Fluids Eng.* **1999**, *121*, 841–849. [CrossRef]
14. Tanaka, T.; Tsukamoto, H. Transient behavior of a cavitating centrifugal pump at rapid change in operating conditions—Part 2: Transient phenomena at pump startup/shutdown. *J. Fluids Eng.* **1999**, *121*, 850–856. [CrossRef]
15. Tanaka, T.; Tsukamoto, H. Transient behavior of a cavitating centrifugal pump at rapid change in operating conditions—Part 3: Classifications of transient phenomena. *J. Fluids Eng.* **1999**, *121*, 857–865. [CrossRef]
16. Lefebvre, P.J.; Barker, W.P. Centrifugal pump performance during transient operation. *J. Fluids Eng.* **1995**, *117*, 123–128. [CrossRef]
17. Wu, D.Z.; Wang, L.Q.; Hu, Z.Y. Experimental study on explicit performance of centrifugal pump during rapid starting period. *J. Eng. Thermophys.* **2006**, *1*, 68–70.
18. Xu, E.; Sun, J.; Chen, X.; Zhao, R. Analysis of internal flow characteristics of the bearingless direct-drive centrifugal pump system during transient start-up. *Processes* **2023**, *11*, 2996. [CrossRef]
19. Dazin, A.; Caignaert, G.; Bois, G. Transient behavior of turbomachineries: Applications to radial flow pump startups. *J. Fluids Eng.* **2007**, *129*, 1436–1444. [CrossRef]
20. Dong, W.; Fan, X.; Dong, Y.; He, F. Transient internal flow characteristics of centrifugal pump during rapid start-up. *Iran. J. Sci. Technol. Trans. Mech. Eng.* **2024**, *48*, 821–831. [CrossRef]
21. Chen, S.Y.; Li, C.F.; Qu, Y.P.; Sui, R.J. Transient hydraulic performance of a centrifugal pump during rapid starting period. *J. Eng. Thermophys.* **2006**, *5*, 781–783.
22. Yun, L.; Bin, L.; Jie, F.; Rongsheng, Z.; Qiang, F. Research on the transient hydraulic characteristics of multistage centrifugal pump during start-up process. *Front. Energy Res.* **2020**, *8*, 76. [CrossRef]

23. Hu, Z.Y.; Wu, D.Z.; Wang, L.Q. Transient hydrodynamic performance of centrifugal pump during rapid starting period: Study of explicit characteristics. *J. Zhejiang Univ. (Eng. Sci.)* **2005**, *39*, 605–608, 622. [CrossRef]
24. Zhang, Y.L.; Ji, Y.Y.; Zhao, Y.J. Deep analysis of the transient behavior of centrifugal pumps during startup and shutdown. *Meas. Control* **2022**, *55*, 155–163. [CrossRef]
25. Shourkaei, H.A. Transient performance during stopping the research reactor primary loop pump. *Kerntechnik* **2015**, *80*, 40–44. [CrossRef]
26. Ma, X.; Liu, J.; Wang, L. Numerical simulation of the transient process of power failure in a mixed pump. *Adv. Mech. Eng.* **2013**, *5*, 743201. [CrossRef]
27. Liu, J.; Li, Z.; Wang, L.; Jiao, L. Numerical simulation of the transient flow in a radial flow pump during stopping period. *J. Fluids Eng.* **2011**, *133*, 111101. [CrossRef]
28. Feng, J.; Ge, Z.; Zhang, Y.; Zhu, G.; Wu, G.; Lu, J.; Luo, X. Numerical investigation on characteristics of transient process in centrifugal pumps during power failure. *Renew. Energy* **2021**, *170*, 267–276. [CrossRef]
29. Liu, Y.; Zhou, J.; Zhou, D. Transient flow analysis in axial-flow pump system during stoppage. *Adv. Mech. Eng.* **2017**, *9*, 1–8. [CrossRef]
30. Zhang, Y.L.; Zhu, Z.C.; Li, W.G.; Xiao, J.J. Effects of viscosity on transient behavior of a low specific speed centrifugal pump in starting and stopping periods. *Int. J. Fluid Mech. Res.* **2018**, *45*, 1–20. [CrossRef]
31. Wu, D.; Wu, P.; Yang, S.; Wang, L. Transient characteristics of a closed-loop pipe system during pump stopping periods. *J. Press. Vessel Technol.* **2014**, *136*, 021301. [CrossRef]
32. Zhang, Y.L.; Zhu, Z.C.; Sheng, Y.N.; Cui, B.L.; Li, Y. Experimental study on a prototype centrifugal pump with open impeller during stopping period. *Int. J. Fluid Mech. Res.* **2016**, *43*, 18–27. [CrossRef]
33. Zhang, Y.L.; Zhu, Z.C.; Li, W.G.; Jia, X.Q. Non-inertial stopping characteristics of a prototype pump. *Adv. Mech. Eng.* **2019**, *11*, 1–15. [CrossRef]
34. Kan, K.; Zheng, Y.; Chen, H.; Zhou, D.; Dai, J.; Binama, M.; Yu, A. Numerical simulation of transient flow in a shaft extension tubular pump unit during runaway process caused by power failure. *Renew. Energy* **2020**, *154*, 1153–1164. [CrossRef]
35. Hou, G.X.; Liu, M.Q.; Liang, X.; Wu, Y. Research on the curve fit of axial flow pump based on neural network. *China Rural. Water Hydropower* **2020**, *8*, 102–104.
36. Huang, R.; Zhang, Z.; Zhang, W.; Mou, J.; Zhou, P.; Wang, Y. Energy performance prediction of the centrifugal pumps by using a hybrid neural network. *Energy* **2020**, *213*, 119005. [CrossRef]
37. Tang, Y.; Xiao, M.; Tang, L.D. Piecewise least squares polynomial curve fitting algorithm for tested pump performance data. *J. Drain. Irrig. Mach. Eng.* **2017**, *35*, 744–748. [CrossRef]
38. Zhang, Y.L.; Zhu, Z.C.; Li, W.G. Experiments on transient performance of a low specific speed centrifugal pump with open impeller. *Proc. Inst. Mech. Eng. Part A J. Power Energy* **2016**, *230*, 648–659. [CrossRef]
39. Zhang, Y.L.; Zhu, Z.C.; Li, W.G.; Zhou, Z.Z.; Xiao, J.J. Hydraulic performance of low specific-speed centrifugal pump with compound impeller during stopping period. *Trans. Chin. Soc. Agric. Eng.* **2018**, *34*, 95–103. [CrossRef]
40. Yang, L.; Liu, S.; Tsoka, S.; Papageorgiou, L.G. A regression tree approach using mathematical programming. *Expert Syst. Appl.* **2017**, *78*, 347–357. [CrossRef]
41. Zhang, C.; Liao, T.T.; Sun, Y.; Meng, X.L.; Zhang, C.Y. Research on refined flow field simulation based on machine learning methods. *Huanjing Kexue Xuebao.* **2022**, *42*, 318–331. [CrossRef]
42. Breiman, L. Random forests. *Mach. Learn.* **2001**, *45*, 5–32. [CrossRef]
43. Liu, B.; Gao, R.; Du, X.; Wang, Y.; Shang, Y.; Zhang, Y.; Zhao, K.; Li, A. Study on a check valve for airducts with a nonmobile guide vane based on a random forest model. *Build. Environ.* **2022**, *219*, 109243. [CrossRef]
44. Liu, Y.Q.; Xiao, F.G.; Chen, C.H. Study on rapid determination method of ash content in wheat flour based on stochastic forest regression model. *Food Mach.* **2024**, *40*, 79–83. [CrossRef]
45. Luo, J.; Fang, Z.D.; Yuan, Q. Research on channel estimation method based on integrated neural network. *J. Chongqing Univ. Posts Telecommun. (Nat. Sci. Ed.)* **2020**, *32*, 969–975. [CrossRef]
46. Zhang, Y.F.; Lu, Z.Q. Remaining useful life prediction based on an integrated neural network. *Chin. J. Eng.* **2020**, *42*, 1372–1380. [CrossRef]

Disclaimer/Publisher's Note: The statements, opinions and data contained in all publications are solely those of the individual author(s) and contributor(s) and not of MDPI and/or the editor(s). MDPI and/or the editor(s) disclaim responsibility for any injury to people or property resulting from any ideas, methods, instructions or products referred to in the content.